15A.3 THE IMPACT OF FUTURE CLIMATE CHANGE ON TROPICAL CYCLONE INTENSITY AND STRUCTURE: A DOWNSCALING STUDY

Kevin A. Hill*, and Gary M. Lackmann
North Carolina State University, Raleigh, North Carolina

1. Introduction

It is recognized that the study of anthropogenic warming influences on tropical cyclone (TC) intensity requires a downscaling approach (e.g., Knutson et al. 2010). High-resolution mesoscale models can be used in conjunction with GCM-derived large-scale changes; this approach is utilized here. Control simulations are produced using current reanalysis data, and the impact of climate change is studied by perturbing this large-scale environment in accordance with GCM-projected changes obtained from an ensemble of IPCC AR4 simulations.

Previous idealized studies have suggested the potential for increased future TC intensity and rainfall, with increases in average central pressure deficit of 14%, and increases in rainfall within 100-km of TC center of 20% (e.g., Knutson and Tuleya 2001, 2004).

The goal of this study is to assess the impact that projected changes in the tropical thermodynamic environment (SST, atmospheric temperature and moisture) would have on maximum TC intensity and structure. This study will advance previous research in several ways:

1. A larger sample of current state-of-the-art GCM projections from three emissions scenarios will be utilized to provide estimates of changes in environmental SST and tropospheric temperature and moisture due to global warming.
2. An increased emphasis will be placed on the physical processes responsible for GCM-projected changes and also changes in TC intensity and structure.
3. TCs are simulated using a convection resolving model configuration, with either 6- or 2-km grid spacing. The omission of a CP scheme allows for the TC secondary circulation to be better resolved, leading to a more realistic structure and a better projection of possible intensity change.

* *Corresponding author address:* Kevin A Hill, Department of Marine, Earth, and Atmospheric Sciences, 1125 Jordan Hall, Box 8208, Raleigh NC 27695-8208. e-mail: kahill@ncsu.edu

2. Methodology

Environmental current climate values in this study were computed using September 1990 – 1999 2.5º NCEP/NCAR reanalysis data averaged over the western half of the Atlantic "Main Development Region" (MDR) (Fig. 1). The horizontally uniform domain SST was calculated from averages of daily high resolution blended SST analyses derived from Advanced Very High Resolution Radiometer (AVHRR) infrared satellite SST data, available on a 0.25° grid (Reynolds et al. 2007).

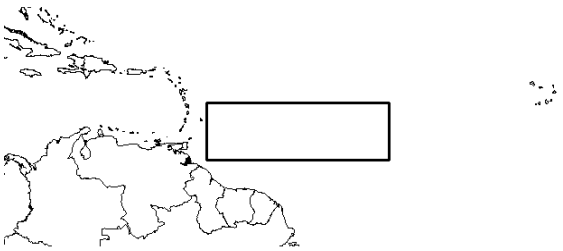

Figure 1. Outline of averaging region. The region encompasses 8.5 – 15º North, and 60 – 40º West.

Future climate conditions were determined using GCM projections conducted for the IPCC Fourth Assessment Report (AR4) with temperature, moisture, and SST data available for 20th century experiments and for 21st century projections using the A1B, B1, and A2 emissions scenarios. These data were available for 13 different GCMs, listed in Table 1. The projected change in each variable was calculated as the difference between the 2090–2099 mean and the 1990–1999 mean, averaged for the region shown in Fig. 1. The 1990–1999 average values were computed using the 20th century simulations. Future climate conditions were calculated by summing the *GCM projected changes* in each variable with the *reanalysis-derived* current climate average.

An axisymmetric TC-like vortex was inserted within each horizontally uniform environment, similar to the procedure used by Hill and Lackmann (2009).

The WRF model version 2.2 (Skamarock et al. 2007) was used to simulate idealized TCs in the different large-scale environments. The model

was run on an actual geophysical domain without land (TC initially centered within the domain at 13°N) and with full model physics. The SST remained constant during the model integrations. A total of 78 model simulations were performed with 6-km grid spacing, while 6 additional experiments were performed with a nested 2-km grid. Simulations with only a 6-km grid were performed using projected changes from individual GCMs, and for each emissions scenario, with 2 combinations of model physics (described below) yielding a total of 78 future simulations. Additional experiments with a 2-km nest within a 6-km parent domain were performed using the current climate conditions or future values computed using the ensemble mean projected changes from each of the 3 selected emissions scenarios. In the vertical, 47 unevenly spaced layers were used, with a higher concentration in the boundary layer.

CMIP3 I.D.	Modeling group and country	Atmospheric Grid Spacing (°)
BCCR-BCM2.0	BCCR, Norway	2.81 x 2.79
CSIRO-Mk3.0	CSIRO, Australia	1.88 x 1.87
CSIRO-Mk3.5	CSIRO, Australia	1.88 x 1.87
CNRM-CM3	CNRM, France	2.81 x 2.79
GFDL-CM2.0	GFDL, USA	2.5 x 2.0
GFDL-CM2.1	GFDL, USA	2.5 x 2.0
INM-CM3.0	INM, Russia	5.0 x 4.0
IPSL-CM4	IPSL, France	3.75 x 2.54
MIROC3.2(medres)	CCSR/NIES/FRCGC, Japan	2.81 x 2.79
ECHAM5	MPI, Germany	1.88 x 1.87
MRI-CGCM2.3.2	MRI, Japan	2.81 x 2.79
CCSM3	NCAR, USA	1.41 x 1.4
UKMO-HadCM3	UKMO, UK	3.75 x 2.5

Table 1. CMIP3 I.D., modeling group and country, and atmospheric grid spacing for GCMs that contained necessary data fields for the 20th century simulation and future simulations with the A1B, A2, and B1 emissions scenarios.

WRF Model simulations featured explicit convection (no CP), either the Mellor-Yamada-Janjic (MYJ) or Yonsei-University (YSU) surface layer/PBL parameterization scheme, the WSM 6-class microphysical scheme, the rapid radiative transfer model (RRTM) longwave and the Goddard shortwave radiation schemes.

3. GCM Projections

In the tropics, increases in CO_2 concentration cause a rise in surface temperature (or over the ocean, SST), which in turn leads to tropospheric lapse rate stabilization (e.g. Rennick 1977; Sobel et al. 2002). Convective processes, parameterized in GCMs, play a key role in these tropospheric temperature changes. Stratospheric processes (see Ramaswamy et al. 2001 for a comprehensive summary) also impact temperature changes in the upper troposphere (e.g., Cordero and Forster 2006; Forster et al. 2007), and could potentially impact TC intensity. Based on the known response of the tropical atmosphere to CO_2 forcing, it is expected that temperature changes in the tropics would to increase with height up to the tropopause. Model-to-model variability in projected temperature increases are expected to increase with height, due to model differences in CP, vertical resolution, and ozone treatment.

Each scenario features a similar profile of temperature change, and the amount of tropospheric stabilization is proportional to the projected SST increase, as a consequence of moist convective adjustment (Fig. 2). Stratospheric cooling is projected, although additional model experiments (not shown) and Shen et al. (2000) indicate that stratospheric cooling has a relatively small influence on TC intensity relative to tropospheric changes.

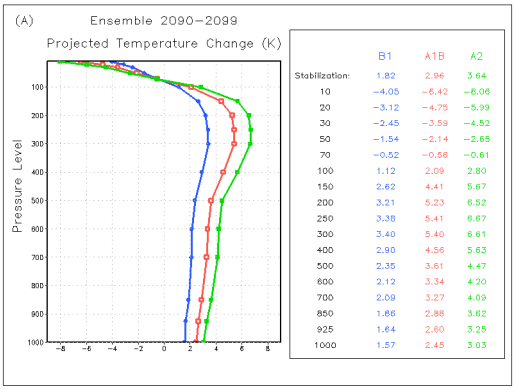

Figure 2. GCM ensemble mean projected change in spatially and temporally averaged temperature (K) for the following emissions scenarios: B1 (blue), A1B (red), and A2 (green). Change is calculated as the difference between the 2090-2099 mean and the 1990-1999 mean, spatially averaged in the region shown in Fig. 1.

GCM projections from each emissions scenario indicate an increase in atmospheric moisture throughout the troposphere, with the largest increases near the surface (not shown). The maximum near-surface moistening in the A2 scenario (3.7 g kg^{-1}) is more than double that in the B1 scenario (1.8 g kg^{-1}) due to the larger warming in A2 and the non-linear relationship between saturation vapor pressure and temperature.

There is considerable variability in projected temperature increase, especially in the upper troposphere (Fig. 3). Part of this variability is due to differences in the projected level of maximum warming. Given the importance of upper level temperature changes on outflow temperature (shown subsequently), this uncertainty needs to be recognized.

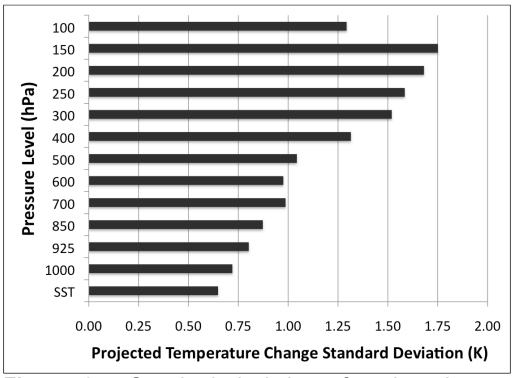

Figure 3. Standard deviation of projected temperature change (K) among all 39 GCM projections as a function of pressure level.

4. TC intensity changes

Maximum TC intensity was assessed by examining the minimum sea level pressure (MSLP) of the simulated TC at each 3-hourly output time.

Combined results for all 78 model runs indicate that 75 of 78 (~96%) future climate simulations indicate an increase in TC intensity, although considerable spread exists (Fig. 4). Two simulations indicate intensity increases of greater than 18%, and 3 simulations (~4%) exhibit future weakening. Environmental changes provided by one GCM (the IPSL model) yield 2 of the 3 future simulations with reduced TC intensity; this GCM also featured the largest tropospheric stabilization (not shown). The largest increase in TC intensity is found using the A1B projection of the BCCR GCM, with a 22% increase in central pressure deficit. The collective results from the 6-km simulations indicate that the most likely increase in future TC intensity is from 9 – 12 %.

Averaged over the individual GCMs, the B1 emissions scenario produces the smallest increase in TC intensity (a 6 hPa decrease in MSLP, or a 8% increase in pressure deficit relative to the ambient environment), while A1B and A2 produce similar increases in TC intensity (8 hPa, 10%). These average percentage increases in pressure deficit are slightly less than the average increase of 14% found by Knutson and Tuleya (2004), although there is clearly a considerable range in the individual simulations, and results with 2-km grid spacing indicate greater future intensification.

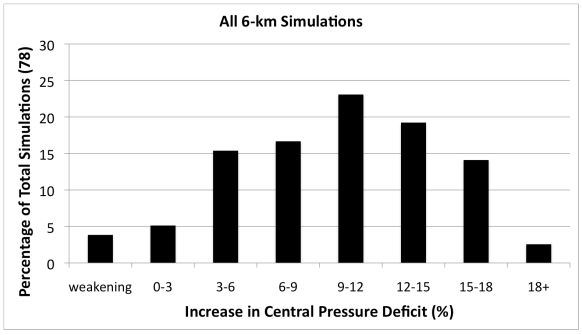

Figure 4. Frequency diagrams illustrating the percentage change in central pressure deficit in future climate simulations with 6-km simulations.

Simulations with 2-km grid spacing utilized the *ensemble mean* projected changes from each emissions scenario to save computational expense. Compared with the 6-km simulations, the 2-km simulations are more intense (Table 2), consistent with previous studies suggesting an increase in simulated TC intensity with increasing resolution (e.g. Hill and Lackmann 2009a; Gentry and Lackmann 2010). Averaged over each model physics combination, increases in central pressure deficit of 11, 19, and 12% are found in the A1B, A2, and B1 simulations, respectively.

PBL parameterization	Large-scale environment	Minimum SLP (hPa)	SLP reduction relative to control (hPa)	Increase in central pressure deficit (%)
MYJ	Current	911		
MYJ	A1B	900	11	11
MYJ	A2	892	19	19
MYJ	B1	894	16	17
YSU	Current	928		
YSU	A1B	916	11	14
YSU	A2	912	16	19
YSU	B1	923	5	6
Average	Current	918		
Average	A1B	908	11	11
Average	A2	902	18	19
Average	B1	909	11	12

Table 2. Summary of maximum intensity and future climate intensity change for simulations with 2-km grid spacing.

5. Precipitation amounts

Averaged over the entire simulation period, increases in future TC rainfall are evident (Fig. 5). Utilizing the 100-km radial averaging distance as in Knutson and Tuleya (2004), increases in average rainfall of 18%, 20%, and 10% are found in the A1B, A2, and B1 simulations, respectively. The values from simulations with A1B and A2 projected changes are similar to Knutson and Tuleya (2004), 18%, while the increase using the B1-projected changes is less, as expected with reduced tropospheric moistening relative to the other scenarios. Further analysis traced the increase in TC rainfall to increased tropospheric water vapor rather than increases in updraft strength.

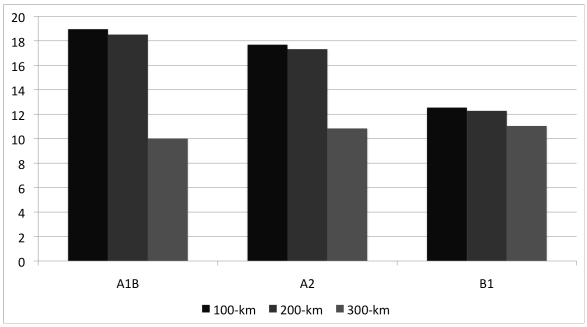

Figure 5. Percentage increase (relative to the control simulation) in area-averaged rainfall rate within various distances of the TC center averaged over the entire simulation period in TC simulations with 2-km grid spacing.

6. TC structure changes

Changes in the thermal structure of the tropospheric environment, and specifically the freezing level, may impact the TC secondary circulation, although to our knowledge previous work has not investigated this possibility in detail. Relative to the control, the outer core freezing level increases by ~700, ~800, and ~400 m in the A1B, A2, and B1 simulations, respectively. The upward shift of the freezing level in future simulations is larger in the TC core than in the ambient environment due to enhanced latent heat release.

A contoured frequency by altitude diagram (CFAD; Fig. 6) demonstrates an upward shift in maximum updrafts from ~4.5 km altitude in the control simulation to between 5.5 and 6 km in future simulations; this increase is comparable to the increase in height of the freezing level in the eyewall. Maximum updraft speeds are ~10 m s^{-1} in all simulations. Above the level of maximum updrafts, stronger upward motion is found in the future simulations relative to the control up to an altitude of 18 km.

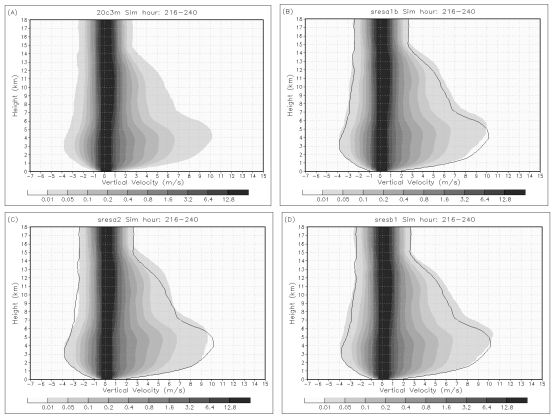

Figure 6. Contoured frequency by altitude diagram of vertical velocity (m s^{-1}) averaged between simulation hours 216 and 240 for: (a) control simulation, (b) A1B, (c) A2, and (d) and B1. In diagrams for the future TC simulations, the 0.01% contour from the control simulation is shown for comparison.

Cross sections of azimuthally averaged temperature and outflow velocity (Fig. 7) demonstrate that while outflow in future simulations occurs at higher altitudes, it is also warmer, as the increased SSTs and subsequent tropospheric stabilization have led to warmer temperatures in the upper troposphere.

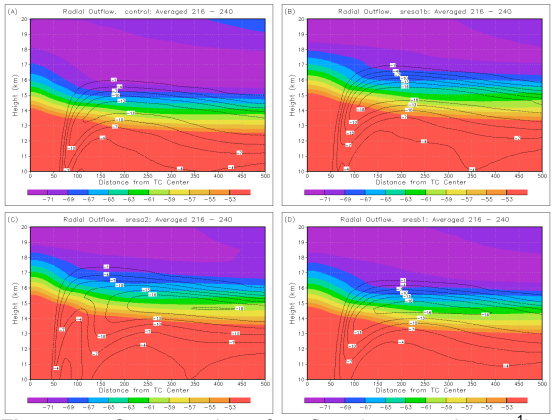

Figure 7. Cross section of outflow (contoured, m s^{-1}) and temperature (shaded, °C) averaged between simulation hours 216 and 240, for: (a) control simulation, (b) A1B, (c) A2, and (d) and B1.

Analysis of outflow mass as a function of temperature (Fig. 8a) indicates a warming of the outflow due to tropospheric stabilization and stronger latent heating in the eyewall; the percentage of outflow mass colder than -59°C is ~95% in the control simulations and ~65% in the A2 simulation (Fig. 8b).

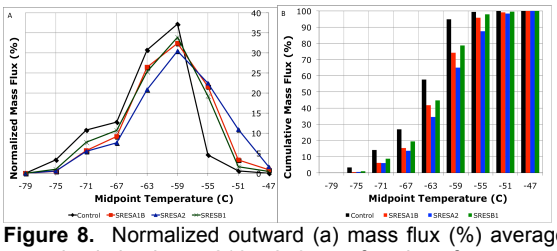

Figure 8. Normalized outward (a) mass flux (%) averaged over simulation hours 216 – 240 as a function of temperature (°C), and cumulative normalized outward mass flux (b). Values restricted to outflow in the 10 – 20 km layer

Overall, the thermodynamic efficiency is similar in the control and A1B simulations, but is reduced in the A2 and B1 future simulations (Table 3). This reduction is attributable to a warmer mass-weighted outflow temperature, and seemingly contradictory to the increased intensity. Despite the lower thermodynamic efficiency in the A2 simulation, the larger amount of tropospheric water vapor and heavier precipitation in this simulation allows for stronger latent heat release and a stronger precipitation mass sink effect (Lackmann and Yablonsky 2004), increased diabatic potential vorticity generation, and subsequently a more intense TC despite the lower thermodynamic efficiency.

Simulation	Inflow Temperature (°C)	Outflow Temperature (°C)	$\frac{T_{in}-T_{out}}{T_{out}}$
Control	21.9	-59.0	0.378
A1B	24.5	-57.1	0.378
A2	25.2	-55.2	0.371
B1	23.6	-57.2	0.374

Table 3. Mass-weighted average inflow temperature, outflow temperature, and thermodynamic efficiency, averaged over simulation hours 216 – 240.

As expected from the increase in precipitation and latent heat release in future simulations, stronger diabatic PV production results in stronger diabatic PV towers in those simulations (Fig. 9), with the strength of the lower-tropospheric portion of the PV tower strongest in the A2 and A1B simulations. This aligns with the TC intensity results, and suggests that the mechanism for stronger TCs in the future is associated with increased diabatic heating and PV production. As discussed by Lackmann and Yablonsky (2004), the precipitation mass sink effect also contributes to PV production. A PV budget would be required to determine the relative importance of increased latent heating and the mass sink effect to the strengthened PV tower in the future simulations.

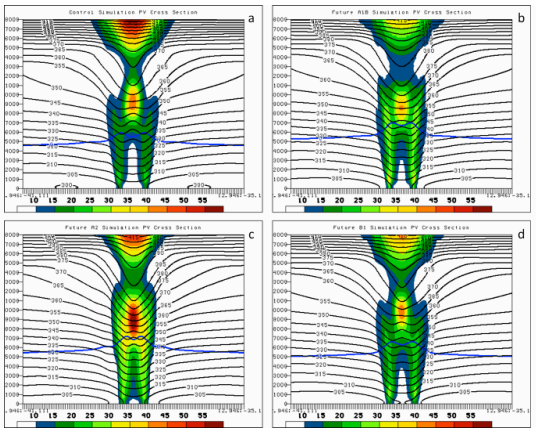

Figure 9. Cross section of time-averaged (simulation hours 216 – 240) azimuthally averaged potential vorticity (shaded; PVU), potential temperature (black contours, K), and the 0° C isotherm (blue contour), for: (a) control simulation, (b) A1B, (c) A2, (d) B1. Cross sections are west-east, and extend 3-degrees of longitude on either side of the TC center.

7. Discussion and Conclusions

In this study, the thermodynamic impact of anthropogenic climate change on maximum TC intensity was investigated. The methodology used here utilizing analyzed data to represent the average environment in which current TCs form, GCM output to assess 21st century changes in SST, air temperature, and moisture, and a high-resolution mesoscale model (WRF) to simulate idealized TCs. This approach is designed to examine changes in the maximum intensity of TCs during time periods which are favorable for strong TC development.

Simulation results with 6-km grid spacing indicate that the most likely increase in central pressure deficit is in the 8-12 hPa range, or 12-16%, relative to the control simulation. Future TC intensity increases were found to be sensitive to emissions scenario with average increases in central pressure deficit of 10, 11, and 5% found in future simulations with A1B, A2, and B1 emissions scenarios, respectively. These results are similar to those of Knutson and Tuleya (2004). Increases in future TC central pressure deficit of 11, 19, and 12% were found in simulations with 2-km grid spacing using the A1B, A2, and B1 emissions scenarios ensemble mean projected changes, or 13% averaged over all 2-km simulations.

The change in TC intensity found in the future simulations is linked to both projected changes

in the atmosphere and ocean; tropospheric lapse-rate stabilization, present in all the GCM projections, plays a role in offsetting the larger increase in intensity that would occur solely based on the projected SST change. Future weakening in a small number of future simulations indicates that an increase in tropospheric stability can completely negate the intensity increase that would occur due to a modest increase in SST, highlighting the importance of the balance between SST increase and tropospheric stabilization. Furthermore, the large standard deviation in the strength of upper-tropospheric warming between the GCM runs reduces confidence in this important aspect of the projected changes in TC intensity.

Rainfall increases within 100-km of the TC center of approximately 19, 20, and 12% in simulations with A1B, A2, and B1 projected changes, respectively, were simulated. These increases are comparable to the 18% found by Knutson and Tuleya (2004), and demonstrate that the increase in rainfall is tied to projected increases in atmospheric water vapor.

Future TCs featured a deeper secondary circulation, with maximum updrafts higher in altitude and updrafts extending higher than in the control. These changes are likely associated with the increase in the height of the freezing level and tropopause, and also increased buoyancy due to higher water vapor content in future climate simulations. Outflow, while occurring at higher altitudes in the future simulations, is warmer than in the control simulation, partially offsetting the increased thermodynamic efficiency that would occur solely due to the increase in inflow temperature. Calculated thermodynamic efficiency, relative to the control simulation, is not larger in future simulations, contradictory to the simulated intensity increase. It appears that the increase in precipitation (related to water vapor increases) in the future climate results in a stronger cyclonic PV tower, warmer eye, and thus a more intense TC despite the lack of increase in thermodynamic efficiency.

Acknowledgements

This research was supported by DOE grant ER64448 and NSF grant ATM-0334427, both awarded to North Carolina State University. We also thank the PCMDI for collecting and archiving the CMIP3 model output, and the WCRP's WGCM for organizing the model data analysis activity. The WCRP CMIP3 multimodel dataset is supported by the Office of Science, U.S. Department of Energy. The WRF model was made available through NCAR, sponsored by the NSF. Model simulations were performed at the Renaissance Computing Institute (RENCI), which is supported by UNC Chapel Hill, NCSU, Duke University, and the state of North Carolina. We thank Dr. Eugene Cordero and his graduate student Sium Tesfai of San Jose State University for discussion of model-to-model sensitivity of upper-tropospheric and lower-stratospheric temperature changes, and for examining chemical GCM output in the tropical region. Dr. Walt Robinson of NC State University is acknowledged for useful discussions.

References

Cordero, E. C., and P. M. de F. Forster, 2006: Stratospheric variability and trends in models used for the IPCC AR4. *Atmos. Chem. Phys.,* **6,** 5369 – 5380.

Forster, P. M., G. Bodeker, R. Schofield, S. Solomon, and D. Thompson, 2007: Effects of ozone cooling in the tropical lower stratosphere and upper troposphere. *Geophys. Res. Lett.,* **34,** 1 – 5.

Gentry, M. S., and G. Lackmann, 2010: Sensitivity of simulated tropical cyclone structure and intensity to horizontal resolution. *Mon. Wea. Rev.,* in press.

Hill, K. A., and G. M. Lackmann, 2009: Analysis of Idealized Tropical Cyclone Simulations using the Weather Research and Forecasting Model: Sensitivity to Turbulence Parameterization and Grid Spacing. *Mon. Wea. Rev.,***137,** 745 – 765.

Hill, K. A., and G. M. Lackmann, 2009: Influence of environmental humidity on tropical cyclone size. *Mon. Wea. Rev.,* **137,** 3294 – 3315.

Hill, K. A., and G. M. Lackmann, 2010: The impact of future climate change on TC intensity and structure: a downscaling approach. Submitted to *J. Climate.*

Knutson, T. R., R. E. Tuleya, W. Shen, and I. Ginis, 2001: Impact of CO_2-induced warming on hurricane intensities as simulated in a hurricane

model with ocean coupling. *J. Climate,* **14,** 2458–2468.

– –, – –, 2004: Impact of CO_2-induced warming on simulated hurricane intensity and precipitation: Sensitivity to the choice of climate model and convective parameterization. *J. Climate,* **17,** 3477–3495.

– –, J. J. Sirutis, S. T. Garner, I. M. Held, and R. E. Tuleya, 2007: Simulation of the recent multi-decadal increase of Atlantic hurricane activity using an 18-km grid regional model. *Bull. Amer. Meteor. Sci., **88,*** 1549–1565.

Knutson, T. R., and Coauthors, 2010: Tropical cyclones and climate change. *Nature Geoscience*, **3,** 157 – 163.

Lackmann, G. M., and R. M. Yablonsky, 2004: The importance of the precipitation mass sink in tropical cyclones and other heavily precipitating systems. *J. Atmos. Sci.,* **61,** 1674 – 1692.

Ramaswamy, V., M.-L. Chanin, J. Angell, J. Barnett, D. Gaffen, M. Gelman, P. Keckhut, Y. Koshelkov, K. Labitzke, J.-J. R. Lin, A. O'Neill, J. Nash, W. Randel, R. Rood, K. Shine, M. Shiotani, and R. Swinbank, 2001: Stratospheric temperature trends: Observations and model simulations. *Rev. Geophys.*, **39**, 72– 122.

Rennick. M. A., 1977: The parameterization of tropospheric lapse rates in terms of surface temperature. *J. Atmos. Sci.,* **34,** 854 – 862.

Reynolds, R. W., T. M. Smith, C. Liu, D. B. Chelton, K. S. Casey, and M. G. Schlax, 2007: Daily high-resolution-blended analyses for sea surface temperature. *J. Climate*, **20,** 5473 – 5496.

Santer, B. D., and Coauthors, 2008: Consistency of modeled and observed temperature trends in the tropical troposphere. *Int. J. Climatol.,* **10.1002/joc.1756.**

Shen, W., R. E. Tuleya, and I. Ginis, 2000: A sensitivity study of the thermodynamic environment on GFDL model hurricane intensity: Implications for global warming. *J. Climate,* **13,** 109–121.

Skamarock, W. C., J. B. Klemp, J. Dudhia, D. O. Gill, D. M. Barker, W. Wang, and J. G. Powers, 2007: A description of the advanced research WRF Version 2. *NCAR Technical Note.*

Sobel, A. H., I. M. Held, and C. S. Bretherton, 2002: The ENSO signal in tropical tropospheric temperature. *J. Climate,* **15,** 2702 – 2706.

Vecchi, G. A., and B. J. Soden, 2007: Increased tropical Atlantic wind shear in model projections of global warming. *Geophys. Res. Lett.,* **34,** 1 – 5.